Full Paper
doi.org/10.1002/chem.202004486

Homogenous catalysis

A Calix[4]arene-Based Cyclic Dinuclear Ruthenium Complex for Light-Driven Catalytic Water Oxidation

Niklas Noll[a] and Frank Würthner*[a, b]

Abstract: A cyclic dinuclear ruthenium(bda) (bda: 2,2′-bipyridine-6,6′-dicarboxylate) complex equipped with oligo(ethylene glycol)-functionalized axial calix[4]arene ligands has been synthesized for homogenous catalytic water oxidation. This novel Ru(bda) macrocycle showed significantly increased catalytic activity in chemical and photocatalytic water oxidation compared to the archetype mononuclear reference $[Ru(bda)(pic)_2]$. Kinetic investigations, including kinetic isotope effect studies, disclosed a unimolecular water nucleophilic attack mechanism of this novel dinuclear water oxidation catalyst (WOC) under the involvement of the second coordination sphere. Photocatalytic water oxidation with this cyclic dinuclear Ru complex using $[Ru(bpy)_3]Cl_2$ as a standard photosensitizer revealed a turnover frequency of 15.5 s^{-1} and a turnover number of 460. This so far highest photocatalytic performance reported for a Ru(bda) complex underlines the potential of this water-soluble WOC for artificial photosynthesis.

Introduction

Since the industrial revolution in the mid-18th century, the economic welfare and growth of our society has been significantly driven by the finite reservoir of fossil fuels, including coal, oil and natural gas.[1,2] To satisfy the growing energy demands of the rapidly increasing world population, the transition to a clean, sustainable and carbon-neutral economy is inevitable.[3–5] In search of alternative energy carriers, a long-standing challenge has been the construction of artificial photosynthetic systems in which solar energy is stored in the chemical bonds of solar fuels originating from abundant resources like water or CO_2.[6–9] In this regard, the thermodynamically demanding oxidation of water to molecular oxygen in a complex four-electron process is a critical bottleneck for the generation of carbon-neutral fuels like hydrogen.[10,11] To enable water oxidation at low overpotentials, however, efficient catalysts are required.[12,13] Accordingly, considerable efforts have been made in the last years to develop water oxidation catalysts (WOCs) based on earth-abundant transition metals (Mn, Fe, Co, Ir and Ru).[14–17]

Ruthenium-based catalysts belong to the earliest and most studied molecular WOCs,[13,17,18] where especially the invention of the Ru(bda) system (bda: 2,2′-bipyridine-6,6′-dicarboxylate)[19–21] enabled catalytic activities that are comparable to those of the natural oxygen-evolving cluster (OEC).[22] The highly versatile Ru(bda) fragment facilitated by axial ligand exchange the isolation of multinuclear Ru complexes including dimers[23–25] and trimers,[26] which showed increased catalytic activities compared to mononuclear complexes due to covalent linkage of the catalytic centers accelerating the underlying bimolecular I2M (interaction of two M-O units) mechanism.[27]

In recent years, many examples reported in the literature have emphasized the role of second coordination sphere effects,[13] that is, π–π interactions,[22,28–33] accessible pendant bases,[34–38] hydrogen bonding,[39–42] and steric effects[39,41,43] on the overall water oxidation mechanism. In this regard, several supramolecular approaches have mainly focused on accelerating the underlying bimolecular I2M mechanism by self-assembly of two catalytic subunits through π–π interactions,[22,28–33] whereas the integration of accessible pendant bases like carboxylates in the second coordination sphere leads to a mechanistic change to the water nucleophilic attack (WNA) pathway due to their ability to act as a intramolecular proton acceptor in the rate-determining step of oxygen bond formation.[34–38] Our group has shown that the incorporation of Ru(bda) units into trimeric metallo-supramolecular macrocycles leads to high catalytic activity in water splitting through the formation of a hydrogen-bonded water network inside the cavity, resulting in a lower activation barrier for water nucleophilic attack by involving the second coordination sphere.[39,41] Kinetic studies indeed confirmed that these trinuclear Ru(bda) macrocycles function through a WNA mechanism.

[a] N. Noll, Prof. Dr. F. Würthner
Institut für Organische Chemie, Universität Würzburg
Am Hubland, 97074 Würzburg (Germany)
E-mail: wuerthner@uni-wuerzburg.de

[b] Prof. Dr. F. Würthner
Center for Nanosystems Chemistry (CNC)
Universität Würzburg, Theodor-Boveri-Weg, 97074 Würzburg (Germany)

Supporting information and the ORCID identification number(s) for the author(s) of this article can be found under: https://doi.org/10.1002/chem.202004486.

Although several noncyclic dinuclear Ru WOCs that exhibit variable catalytic activities involving the I2M mechanism have been reported in the literature,[23–26] studies on catalytic water oxidation with cyclic dinuclear Ru complexes are barely known and only in a patent have the synthesis and X-ray crystal structure analysis of such cyclic complexes, but no catalytic activities, been reported.[44] Motivated by the fact that cyclic complexes are structurally by far more preorganized than the previously investigated noncyclic dinuclear systems, and indeed the high catalytic activities of our previously reported trinuclear Ru(bda) macrocycles, we have now designed a cyclic dinuclear complex by employing an axial calix[4]arene ligand for catalytic water oxidation involving the second coordination sphere.

Due to the poor water solubility of unmodified calix[4]arenes,[45] the hydrophilic narrow lower rim of the ligand was functionalized with four tri(ethylene glycol) chains. In combination with two phenylpyridine units, substituted at the hydrophobic wider upper rim, the calix[4]arene ligand was conformationally fixed in its cone conformation.[46] A large variety of calix[*n*]arenes have been applied as ancillary ligands in metal-based catalysis,[47] whereas to date only one example of a calix[4]arene-based mononuclear Ru(bda) complex is reported for catalytic water oxidation with rather poor performance (turnover number (TON) = 762, turnover frequency (TOF) not reported)[48] and, to the best of our knowledge, cyclic dinuclear Ru complexes based on calix[*n*]arenes are so far unprecedented.

Herein, we report the synthesis of a novel cyclic dinuclear Ru(bda) complex **dimer 1** containing functionalized calix[4]arene axial ligands that exhibits high catalytic activities in both chemical and photocatalytic water oxidation. Our kinetic studies revealed that this macrocyclic WOC operates by a WNA mechanism. Under highly diluted conditions, this dinuclear Ru(bda) complex performed outstanding photocatalytic water oxidation with a TOF value of 15.5 s^{-1}, which makes **dimer 1** the most active homogenous Ru(bda) catalyst for light-driven water oxidation reported in literature to date.

Results and Discussion

Synthesis, electrochemical and spectroscopic studies of dimer 1

The dinuclear calix[4]arene-based cyclic Ru complex **dimer 1**, bearing eight tri(ethylene glycol) chains as water-solubilizing groups, was synthesized according to the route depicted in Scheme 1. The solubilizing groups were incorporated into the axial calix[4]arene-based ligand **9** in five steps by literature adapted procedures,[49–51] starting from commercially available 4-*tert*-butylcalix[4]arene **1**. The target Ru complex **dimer 1** was then synthesized through a ligand exchange reaction of the precursor [Ru(bda)(dmso)$_2$] **10**[52] with the phenylpyridine-functionalized calix[4]arene ligand **9** in a chloroform/methanol mixture under a nitrogen atmosphere. Purification of the crude product by column chromatography afforded the desired dinuclear complex **dimer 1** in 50% isolated yield. The structures of **dimer 1** and all unknown precursors were elucidated by 1D and 2D NMR spectroscopy and high-resolution mass spectrometry. The purity of the compounds were confirmed by elemental analysis. Detailed synthetic procedures and characterization data of all new compounds are reported in the Supporting Information. Semiempirical PM6 calculations (for details see the Supporting Information) suggested that in the lowest energy, geometry-optimized structure (Figure S3 in the Supporting Information) both Ru centers are directed into the interior of the cavity of the macrocycle. To further confirm the size of the dimeric structure diffusion-ordered spectroscopy (DOSY) was performed, revealing a hydrodynamic radius of $r = 13.8$ Å (Fig-

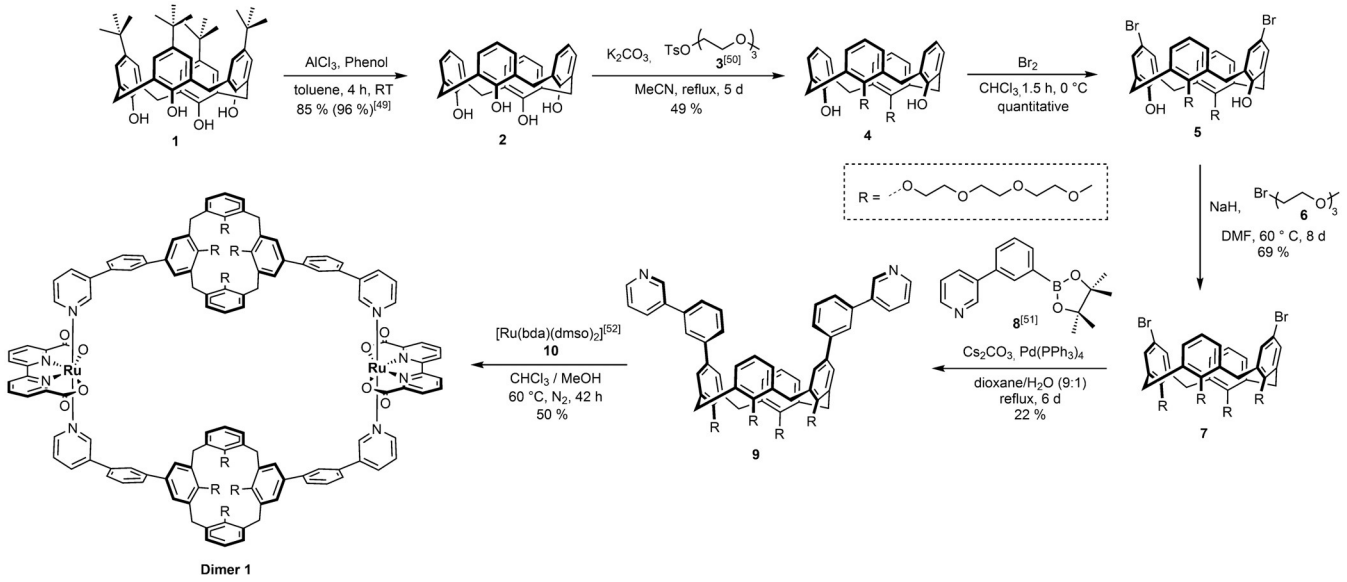

Scheme 1. Synthesis of the target dinuclear calix[4]arene Ru complex **dimer 1**. Boronic ester **8** was prepared in two steps starting from the respective pyridine boronic acid according to ref. [50].

ure S4). The obtained value matches very well with the calculated distance between the two Ru(bda) centers ($d = 27.6$ Å) of the geometry-optimized structure of **dimer 1** (Figure S3).

Electrochemical studies of **dimer 1** were performed by cyclic voltammetry (CV) and differential pulse voltammetry (DPV) in aqueous solution under acidic (pH 1, triflic acid) and neutral conditions (pH 7, phosphate buffer) containing 40% 2,2,2-trifluorethanol (TFE) as a non-coordinating co-solvent for solubilization. The redox properties of **dimer 1** under the applied experimental conditions are summarized in Table S2 and compared with those of the mononuclear reference complex [Ru(bda)(pic)$_2$], and the voltammograms are displayed in Figures S5–S8.[22,53] In acidic aqueous solution (pH 1), **dimer 1** displayed two subsequent oxidation processes which can be assigned to the Ru_2^{III}/Ru_2^{II} and Ru_2^{IV}/Ru_2^{III} redox couples for each metal center in accordance to the redox processes reported for [Ru(bda)(pic)$_2$] (Figure S5 and S6).[22] Due to the overlap with the water oxidation current, the oxidation to Ru_2^{V} could not be observed as it has previously been described for other dinuclear non-cyclic Ru complexes.[23,24] Under neutral conditions (pH 7), three two-electron oxidation events were observed for **dimer 1** which correspond to the oxidation potentials Ru_2^{III}/Ru_2^{II}, Ru_2^{IV}/Ru_2^{III} and Ru_2^{V}/Ru_2^{IV} for each metal center (Figure S7). Compared to the mononuclear complex [Ru(bda)(pic)$_2$], the incorporation of the axial calix[4]arene in **dimer 1** affected under both acidic and neutral conditions only the Ru_2^{III}/Ru_2^{II} redox potential, resulting in an approximately 50 mV higher oxidation potential for this dinuclear cyclic Ru(bda) complex.

The UV/Vis absorption spectra of **dimer 1** at the Ru_2^{II} state under both acidic and neutral conditions displayed a very strong absorption band at around 250 nm, which belongs to an electronic transition along the long molecular axis (^1L_a) for the axial calix[4]arene ligand (Figure S9).[54] The transition along the short molecular axis (^1L_b) of the calix[4]arene ligand is usually very weak and is presumably overlapping with the ligand centered π–π* transitions at around 300 nm.[55] The weak absorption bands in the visible region can be attributed to several metal-to-ligand charge transfer (MLCT) absorptions,[56,57] where the band at around 360 nm is characteristic for the transition from the Ru d-orbital to the π*-orbital of the axial ligand, while the less energetic bands at 450 and 500 nm can be explained by the transition from the Ru d-orbital to the π*-orbital of the equatorial bda ligand.[41] Compared to the mononuclear [Ru(bda)(pic)$_2$], the high-energy MLCT band at 360 nm is bathochromically shifted for **dimer 1** indicating a less donating character of the axial calix[4]arene ligand.[57]

To investigate the spectral changes of **dimer 1** upon oxidation, spectroelectrochemistry in CH_3CN/H_2O 4:6 at pH 7 (phosphate buffer) was performed (Figure 1). Upon increasing the potential from 500 mV to approximately 800 mV, the MLCT bands at 350 nm and 450–500 nm are bleached with concomitant appearance of a new band at 700 nm which is characteristic for the Ru_2^{III} state.[41,43] A further increase of the potential to approximately 960 mV results in a decrease of the transition at 700 nm and a broad absorption at around 520 nm arises for the formation of the Ru_2^{IV} state (Figures 1 and S10).[43] No further spectral changes were observed upon increasing the potential because a strong catalytic current is associated with the formation of Ru^{V} and subsequent oxidation of water.[39,41]

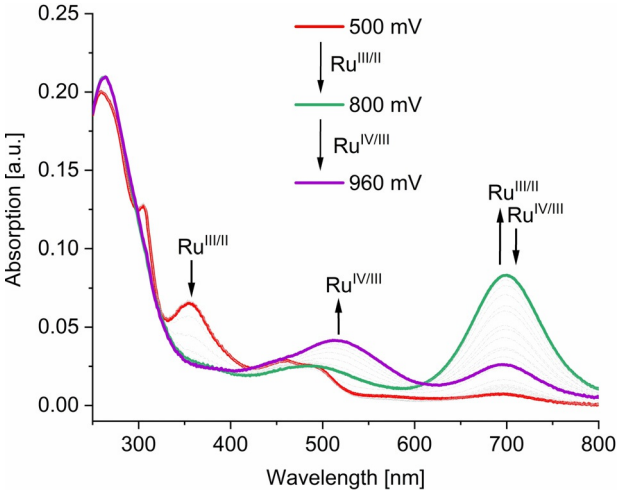

Figure 1. Spectroelectrochemistry of **dimer 1** in CH_3CN/H_2O (4:6; pH 7, phosphate buffer) at $c = 2.4 \times 10^{-4}$ M. The applied voltages for the generation of Ru_2^{II} (red), Ru_2^{III} (green) and Ru_2^{IV} (purple) are indicated.

Chemical water oxidation under acidic conditions

The catalytic performance of **dimer 1** was first investigated in the presence of cerium ammonium nitrate (CAN) as a sacrificial oxidant in aqueous acidic solutions (pH 1, triflic acid) with 40% acetonitrile as co-solvent due to its oxidative stability.[58,59] A large excess of CAN was applied in these experiments to ensure a direct dependence of the overall catalytic rate on the catalyst concentration.[19] After the injection of the catalyst solution into the acidic CAN mixture, the subsequent pressure increase due to oxygen evolution was monitored by the attached pressure sensors. The gas composition at the end of each run was then analyzed by gas chromatography (GC; for experimental details and reaction conditions see the Supporting Information). The catalytic performance of **dimer 1** was then screened in different acetonitrile/water ratios to determine the optimal experimental conditions (Figure S11a). The amount of acetonitrile used as co-solvent strongly correlates with the overall catalytic activity, which can be attributed to its competitive binding to the seventh coordination site of the ruthenium center compared with water.[58,60] For **dimer 1** the highest catalytic activity was achieved in aqueous mixtures containing 40% acetonitrile, whereas higher acetonitrile content led to lower catalytic activity in the initial first two seconds of catalytic water oxidation (Figure S11b). Hence, all further catalytic experiments were performed in CH_3CN/H_2O 4:6 solvent mixtures and compared to the mononuclear complex [Ru(bda)(pic)$_2$][22] under the same conditions.

Concentration-dependent water oxidation experiments were conducted to determine the turnover number (TON) and the turnover frequency (TOF) for the dinuclear cyclic complex **dimer 1** and [Ru(bda)(pic)$_2$] as a mononuclear reference under

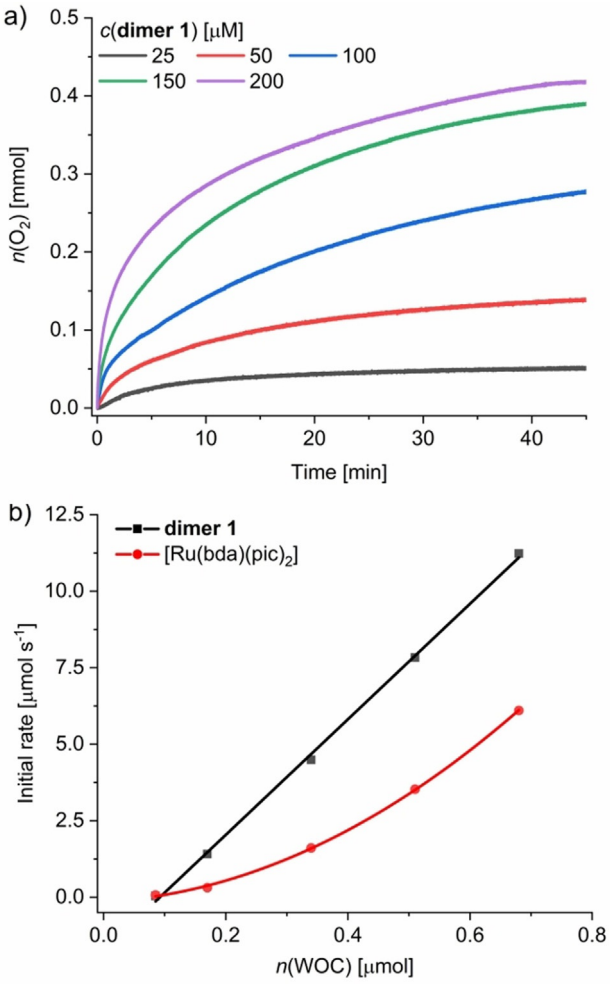

Figure 2. a) Oxygen evolution curves for **dimer 1** at various concentrations in CH_3CN/H_2O (4:6; pH 1, triflic acid), c(CAN) = 0.6 M. b) Concentration-dependent initial rates for **dimer 1** vs. [Ru(bda)(pic)$_2$], including linear regression for the determination of averaged TOF for **dimer 1**.

identical experimental conditions (Figures 2b and S12). The oxygen evolution for both catalysts was detected in the range of 25–200 μM of catalyst concentration (Figures 2a, S12, and S13) and afterwards the initial rates of catalysis were evaluated within the first seconds of catalysis at different catalyst loadings. Notably, the analysis of the head space of each catalytic reaction by gas chromatography confirmed that oxygen was the only gaseous product detected during catalysis with **dimer 1** (Figure S14). As clearly shown in Figure 2b, a linear dependency on the catalyst concentration is observed for **dimer 1** which is indicative of a first-order reaction kinetic in the rate-determining step (RDS) of oxygen evolution according to a WNA mechanism.[39–41] In contrast, mononuclear complex [Ru(bda)(pic)$_2$] displayed a second-order dependency on the catalyst concentration in accordance with the reported bimolecular I2M reaction mechanism (Figure 2b).[21,22,53] In case of a linear relationship, as found for **dimer 1**, the slope of the linear regression represents the averaged TOF value of the catalyst, whereas for a second-order dependency TOF values for each catalyst concentration is calculated. Under optimized conditions, **dimer 1** displayed an averaged TOF of 19 ± 0.5 s^{-1} (~9.5 s^{-1} per Ru unit) while for the mononuclear [Ru(bda)(pic)$_2$] an averaged TOF could not be determined and thus concentration-dependent TOF values of 0.9–9 s^{-1} in the catalyst concentration range from 25–200 μM are shown (Figure 2b). These results clearly show that **dimer 1** is a more efficient WOC than the mononuclear reference with substantial benefit, in particular, at lower concentrations.

Post-catalytic analysis of the reaction mixture of **dimer 1** by HR ESI mass spectrometry indicated oxidative decomposition of the methylene bridges between the aryl units of the axial calix[4]arene ligands (Figure S15). Such oxidative decomposition of methylene groups has been reported previously in literature.[61–63] Thus, we assume that axial ligand exchange of the Ru(bda) WOC,[22] combined with oxidative decomposition of the calix[4]arene ligand in **dimer 1** under acidic conditions, is the main catalyst deactivation pathway. These findings are in accordance with the somewhat lower stability of the cyclic **dimer 1** containing axial calix[4]arene ligands compared to [Ru(bda)(pic)$_2$] as TONs of 760 ± 60 (~380 per Ru unit) and 880 ± 20, respectively, were observed. To get some insights into the reaction kinetics of the underlying water oxidation mechanism of the new WOC **dimer 1**, further experiments in the presence of stoichiometric amounts of cerium ammonium nitrate (CAN) were carried out (for experimental details see the Supporting Information, especially Figures S16 and S17). Thus, the characteristic decay of the CAN absorption band at 360 nm after addition of the catalyst was monitored by UV/Vis spectroscopy over time.[41,64] To study the dependency of the catalytic reaction rate on both components, two different types of experiments were conducted. In a first experiment at a constant CAN concentration, the initial reaction rates at varying catalyst concentration (Figure S16) showed a linear dependency on the catalyst concentration which is in proper accordance with the results of the previous experiments using CAN in large excess (Figure 2). In a second experiment, the catalyst concentration was kept constant and only the oxidant concentration was varied (Figure S17). Under these conditions, **dimer 1** exhibited a linear dependency of the reaction rate on the CAN concentration. Accordingly, an oxidation process from Ru^{IV}-OH to Ru^{V}=O has to be involved in the rate-determining step (RDS) of the oxygen evolution as it has been previously reported for the trinuclear macrocycle **MC3** by our group.[39]

To further explore the mechanism of catalytic water oxidation with **dimer 1**, kinetic isotope effect (KIE) of **dimer 1** and monomeric complex [Ru(bda)(pic)$_2$] were studied in a comparative manner by focusing on possible involvement of an element-hydrogen bond breaking in the RDS of the catalytic process.[65–68] The WNA pathway is characterized by a primary kinetic isotope effect when a direct O-H/D bond cleavage takes place and shows a difference in the reaction rates of at least two (KIE ≥ 2).[68,69] If the RDS involves a dimerization of two Ru=O units, the reaction shows a secondary isotope effect (KIE = 0.7–1.5).[69] Therefore, catalytic water oxidation experiments for both catalysts were conducted in aqueous mixtures (H_2O and D_2O, pH 1, triflic acid) with 40% acetonitrile in the presence of CAN as sacrificial oxidant and a Clark electrode for

O_2 detection (Figures S18, S19). The reaction rates in H_2O ($k(H_2O)$) and D_2O ($k(D_2O)$) for each catalyst were determined from the slope of a linear regression of the initial rates vs. the catalyst amount at different concentrations. For **dimer 1**, a KIE value of 1.8 was obtained due to a significantly reduced reaction rate in heavy water ($k(D_2O) = 2.4\ s^{-1}$) compared to normal water ($k(H_2O) = 4.2\ s^{-1}$). In contrast, the mononuclear complex [Ru(bda)(pic)$_2$] displayed an expected second-order dependency on the catalyst amount (Figure S19b). The reaction rates were determined by plotting the initial rates vs. the square of catalyst amount for linearization of the rate dependency (Figure S19c). The linear regression revealed a secondary isotope effect with a KIE of 0.9 for [Ru(bda)(pic)$_2$], providing evidence for no proton involvement in the RDS of oxygen evolution. The higher KIE value for **dimer 1** is strongly supportive for a primary isotope effect and a mechanistic change from the mostly observed I2M mechanism for Ru(bda) complexes[21] to the WNA mechanism involving a nucleophilic attack of water. As previously shown for a series of Ru(dba) macrocycles of different sizes,[41] small structural changes in the ring size can lead to significant changes of the proton coupling and thus in the KIE.[70] The slightly lower KIE value of 1.8 for **dimer 1** can be taken as an indication for a not fully concerted proton-coupled oxidation of Ru^{IV}-OH to Ru^{V}=O. Thus, we propose a stepwise oxidation process characterized by an initial oxidation to Ru^{V}-OH followed by subsequent deprotonation to Ru^{V}=O.[71–73]

Photocatalytic water oxidation under neutral conditions

To assess the suitability of the catalyst **dimer 1** for potential application in an artificial photosynthetic cell,[9] **dimer 1** was investigated under the conditions of photocatalytic water oxidation with the milder oxidant $[Ru(bpy)_3]^{3+}$, which is photogenerated in situ from the common photosensitizer (PS) [Ru(bpy)$_3$Cl$_2$], in the presence of $Na_2S_2O_8$ as sacrificial electron acceptor (Figures 3 and 4).[74–76] For the purpose of comparison, mononuclear [Ru(bda)(pic)$_2$] was also investigated under identical conditions. Irradiation was performed with a xenon lamp ($I = 100\ mW\,cm^{-2}$; Figure S20) and a Clark electrode was used to detect the generated oxygen. Photocatalytic water oxidation was studied in phosphate buffer at pH 7 containing 40% acetonitrile in accordance with the experiments performed for chemical water oxidation. The concentration of PS (c([Ru(bpy)$_3$Cl$_2$]) = 1.5 mM) and electron acceptor ($c(Na_2S_2O_8)$ = 37 mM) were kept constant and only the concentration of the catalyst was varied for each experiment (for experimental details see the Supporting Information). As depicted in Figure 4a, the oxygen evolution curves of **dimer 1** showed no gas evolution in the dark but after light exposure a linear part in each curve is observed, where the initial rates of catalysis between 55–70 s were determined. The initial rates are hereby limited by the oxidized photosensitizer (PS^+),[77] together with the general complexity of the water oxidation reaction under photocatalytic conditions.[75,78,79] The linear regression in the plot of the initial rates vs. the amount of catalyst revealed a first-order reaction rate for **dimer 1** (Figure 4b). The catalytic activity of the latter could be observed down to a nanomolar concentration regime (12–200 nM), where a remarkably high averaged TOF value of $15.5 \pm 0.3\ s^{-1}$ (~$7.5\ s^{-1}$ per Ru unit) and a TON of 460 ± 20 (~230 per Ru unit) was obtained. Further, the

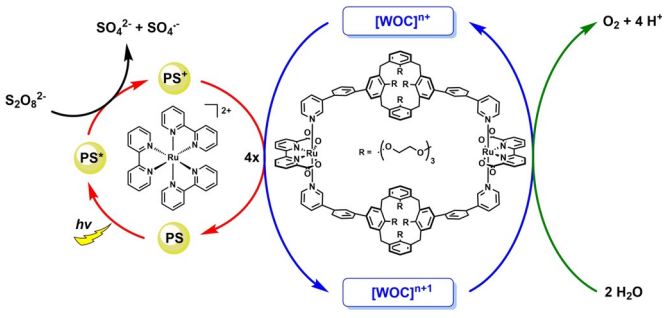

Figure 3. Schematic presentation of the photocatalytic water oxidation cycle in a three-component system containing $Na_2S_2O_8$ as sacrificial electron acceptor, $[Ru(bpy)_3]^{2+}$ as photosensitizer (PS), and **dimer 1** as WOC.

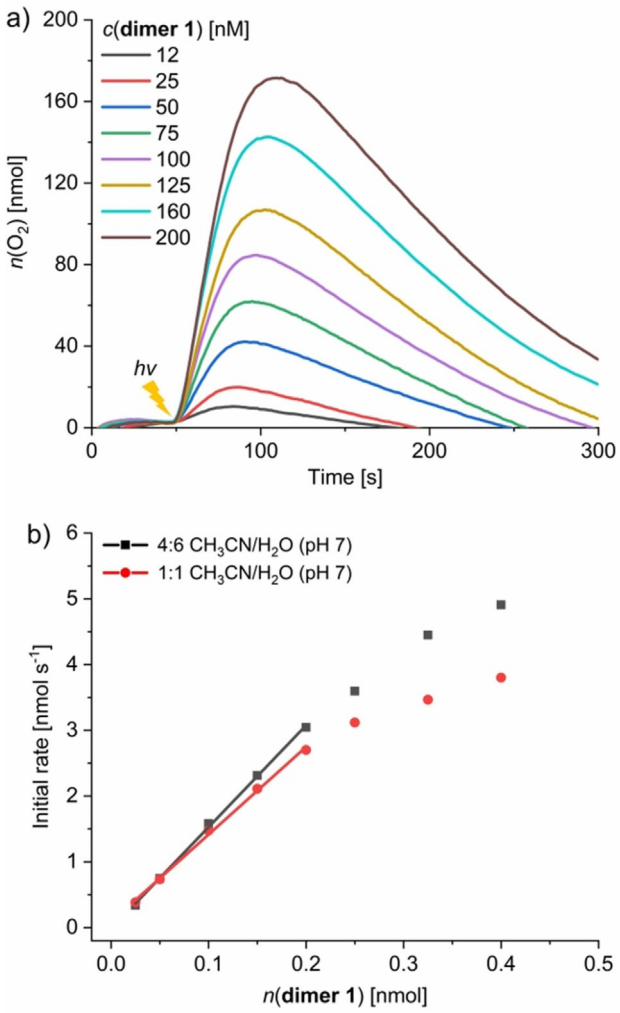

Figure 4. a) Concentration-dependent oxygen evolution curves of **dimer 1** in CH_3CN/H_2O (4:6; pH 7, phosphate buffer), c(PS) = 1.5 mM, $c(Na_2S_2O_8)$ = 37 mM. The lighting symbol indicates the start of sample irradiation at t = 50 s. b) Initial rates for **dimer 1** at different acetonitrile contents with linear regression for the determination of averaged TOF.

influence of acetonitrile on the overall catalysis was investigated by repeating the experiment for **dimer 1** in 1:1 CH_3CN/H_2O (pH 7) mixtures (Figures 4b and S21) resulting in a decreased catalytic activity (TOF = 13.3 ± 0.3 s^{-1} (~6.5 s^{-1} per Ru unit)) and a slightly increased stability (TON = 540 ± 20 (~270 per Ru unit)). These findings are in accordance with the previously reported competitive binding ability of acetonitrile, leading to a decrease in catalytic activity.[25,77] A catalytic sample of the dinuclear complex **dimer 1** was studied before and after catalysis by UV/Vis absorption spectroscopy (Figure S24), which showed a considerable degradation of the photosensitizer at the end of catalysis. For the mononuclear complex [Ru(bda)$(pic)_2$], a higher concentration regime (2.5–20 μM) had to be applied as no catalytic activities could be observed at lower concentrations in the nM regime. Even at higher concentration range (2.5–20 μM), a very low catalytic performance (TOF = 0.1–0.45 s^{-1}, TON = 30 ± 10) was observed for the mononuclear reference (Figure S22).

These studies reveal an outstanding performance of our novel dinuclear cyclic WOC **dimer 1** in photocatalytic water oxidation with a TOF of 15.5 s^{-1} which is indeed so far unprecedented for dinuclear homogenous ruthenium WOCs and even superior to our previously reported highly active trinuclear macrocyclic Ru catalysts[43] (see Table S3 for a comparison of the TOF and TON values of selected mono-, di- and trinuclear Ru WOCs). Usually, significantly higher catalytic values are observed for chemical water oxidation compared with photocatalytic oxidation due to the lower stability and general complexity of the photocatalytic system,[75,79] which is explained based on the limited stability of the photosensitizer.[78,81] In the case of **dimer 1**, however, the difference between the chemical and photocatalytic activities (TOF_{Chem} = 19 ± 0.5 s^{-1}, TON_{Chem} = 760 ± 60; TOF_{Photo} = 15.5 ± 0.3 s^{-1}, TON_{Photo} = 460 ± 20) are comparably small. We attribute this to the higher stability of the dinuclear complex under neutral (photocatalysis) compared to the strong acidic (chemical oxidation) conditions, as it is evidenced by post-catalytic mass spectrometry studies (Figure S15). Further, the photocatalytic activity of **dimer 1** could be improved in aqueous mixtures with lower MeCN content ($TOF_{40\%\ MeCN}$ = 15.5 ± 0.3 s^{-1}; $TOF_{50\%\ MeCN}$ = 13.3 ± 0.3 s^{-1}) as the ability of acetonitrile to competitively bind to the seventh coordination site of the ruthenium center is reduced at lower co-solvent content.[58,60] These results are also in line with a reduced solvation of the photosensitizer at lower amounts of organic co-solvent in CH_3CN/H_2O mixtures, which leads to a more efficient generation of photooxidant PS^+ by quenching with sodium persulfate ($Na_2S_2O_8$; Figure 3).[82]

Conclusions

We have applied one of the most versatile and easily accessible supramolecular hosts, that is, calix[4]arene, as a scaffold for the assembly of a cyclic dinuclear Ru(bda) complex **dimer 1** for catalytic water oxidation. Due to the easy functionalization of the calix[4]arenes with four tri(ethylene glycol) chains at the narrow rim, sufficient water solubility is provided for catalytic water oxidation in the nanomolar concentration regime. Our detailed studies revealed a linear dependency of the reaction rate in catalytic water oxidation with the dinuclear Ru(bda) complex on the catalyst concentration. This was further supported by kinetic experiments and kinetic isotope effect studies, confirming that the catalytic rate depends linearly on the catalyst and oxidant concentration in chemical oxidation. Accordingly, the newly synthesized cyclic dinuclear complex **dimer 1** demonstrates another example of the influence of the second coordination sphere on the catalytic mechanism, where the cyclic ligand environment for Ru(bda) complexes leads to a mechanistic change from a bimolecular I2M mechanism to a unimolecular WNA pathway.[13,17,21,38,39] The calix[4]arene-based cyclic WOC allowed the investigation of catalytic activity under highly diluted conditions;[39] this is highly beneficial for photocatalytic water oxidation in which **dimer 1** reached an unprecedently high catalytic activity for Ru(bda) WOCs with a TOF of 15.5 ± 0.3 s^{-1}.

Acknowledgements

This project has received funding from the European Research Council (ERC) under the European Union's Horizon 2020 Research and Innovation Program (grant agreement no. 787937). The authors thank Maximilian Roth for synthetic support. Open access funding enabled and organized by Projekt DEAL.

Conflict of Interests

The authors declare no conflict of interests.

Keywords: artificial photosynthesis · homogenous catalysis · photocatalysis · ruthenium complexes · water oxidation

[1] A. K. Ringsmuth, M. J. Landsberg, B. Hankamer, *Renew. Sust. Energy Rev.* **2016**, *62*, 134–163.
[2] International Energy Agency (IEA), *World Energy Outlook 2017: Executive Summary* **2017**, *France*.
[3] G. W. Brudvig, S. Campagna, *Chem. Soc. Rev.* **2017**, *46*, 6085–6087.
[4] V. Balzani, A. Credi, M. Venturi, *ChemSusChem* **2008**, *1*, 26–58.
[5] N. Armaroli, V. Balzani, *Chem. Eur. J.* **2016**, *22*, 32–57.
[6] L. Hammarström, *Acc. Chem. Res.* **2015**, *48*, 840–850.
[7] P. D. Frischmann, K. Mahata, F. Würthner, *Chem. Soc. Rev.* **2013**, *42*, 1847–1870.
[8] S. Berardi, S. Drouet, L. Francas, C. Gimbert-Suriñach, M. Guttentag, C. Richmond, T. Stoll, A. Llobet, *Chem. Soc. Rev.* **2014**, *43*, 7501–7519.
[9] B. Zhang, L. Sun, *Chem. Soc. Rev.* **2019**, *48*, 2216–2264.
[10] W. Rüttinger, G. C. Dismukes, *Chem. Rev.* **1997**, *97*, 1–24.
[11] H. Dau, C. Limberg, T. Reier, M. Risch, S. Roggan, P. Strasser, *ChemCatChem* **2010**, *2*, 724–761.
[12] J. Hessels, R. J. Detz, M. T. M. Koper, J. N. H. Reek, *Chem. Eur. J.* **2017**, *23*, 16413–16418.
[13] R. Matheu, M. Z. Ertem, C. Gimbert-Suriñach, X. Sala, A. Llobet, *Chem. Rev.* **2019**, *119*, 3453–3471.
[14] V. Artero, M. Fontecave, *Chem. Soc. Rev.* **2013**, *42*, 2338–2356.
[15] J. D. Blakemore, R. H. Crabtree, G. W. Brudvig, *Chem. Rev.* **2015**, *115*, 12974–13005.
[16] M. D. Kärkäs, B. Åkermark, *Dalton Trans.* **2016**, *45*, 14421–14461.
[17] V. Kunz, D. Schmidt, M. I. S. Röhr, R. Mitrić, F. Würthner, *Adv. Energy Mater.* **2017**, *7*, 1602939.
[18] R. Matheu, P. Garrido-Barros, M. Gil-Sepulcre, M. Z. Ertem, X. Sala, C. Gimbert-Suriñach, A. Llobet, *Nat. Rev. Chem.* **2019**, *3*, 331–341.

[19] R. Staehle, L. Tong, L. Wang, L. Duan, A. Fischer, M. S. G. Ahlquist, L. Sun, S. Rau, *Inorg. Chem.* **2014**, *53*, 1307 – 1319.
[20] L. Duan, L. Wang, F. Li, F. Li, L. Sun, *Acc. Chem. Res.* **2015**, *48*, 2084 – 2096.
[21] B. Zhang, L. Sun, *J. Am. Chem. Soc.* **2019**, *141*, 5565 – 5580.
[22] L. Duan, F. Bozoglian, S. Mandal, B. Stewart, T. Privalov, A. Llobet, L. Sun, *Nat. Chem.* **2012**, *4*, 418 – 423.
[23] Y. Jiang, F. Li, B. Zhang, X. Li, X. Wang, F. Huang, L. Sun, *Angew. Chem. Int. Ed.* **2013**, *52*, 3398 – 3401; *Angew. Chem.* **2013**, *125*, 3482 – 3485.
[24] Z. Liu, Y. Gao, M. Zhang, J. Liu, *Inorg. Chem. Commun.* **2015**, *55*, 56 – 59.
[25] F. Li, C. Xu, X. Wang, Y. Wang, J. Du, L. Sun, *Chin. J. Catal.* **2018**, *39*, 446 – 452.
[26] L. L. Zhang, Y. Gao, Z. Liu, X. Ding, Z. Yu, L. Sun, *Dalton Trans.* **2016**, *45*, 3814 – 3819.
[27] J. Nyhlén, L. Duan, B. Åkermark, L. Sun, T. Privalov, *Angew. Chem. Int. Ed.* **2010**, *49*, 1773 – 1777; *Angew. Chem.* **2010**, *122*, 1817 – 1821.
[28] L. Duan, C. M. Araujo, M. S. G. Ahlquist, L. Sun, *Proc. Natl. Acad. Sci. USA* **2012**, *109*, 15584 – 15588.
[29] B. Li, F. Li, S. Bai, Z. Wang, L. Sun, Q. Yang, C. Li, *Energy Environ. Sci.* **2012**, *5*, 8229 – 8233.
[30] L. Wang, L. Duan, Y. Wang, M. S. G. Ahlquist, L. Sun, *Chem. Commun.* **2014**, *50*, 12947 – 12950.
[31] C. J. Richmond, R. Matheu, A. Poater, L. Falivene, J. Benet Buchholz, X. Sala, L. Cavallo, A. Llobet, *Chem. Eur. J.* **2014**, *20*, 17282 – 17286.
[32] S. Zhan, D. Mårtensson, M. Purg, S. C. L. Kamerlin, M. S. G. Ahlquist, *Angew. Chem. Int. Ed.* **2017**, *56*, 6962 – 6965; *Angew. Chem.* **2017**, *129*, 7066 – 7069.
[33] Y. Xie, D. W. Shaffer, J. J. Concepcion, *Inorg. Chem.* **2018**, *57*, 10533 – 10542.
[34] M. Yoshida, M. Kondo, S. Torii, K. Sakai, S. Masaoka, *Angew. Chem. Int. Ed.* **2015**, *54*, 7981 – 7984; *Angew. Chem.* **2015**, *127*, 8092 – 8095; *Angew. Chem.* **2015**, *127*, 8092 – 8095.
[35] N. Song, J. J. Concepcion, R. A. Binstead, J. A. Rudd, A. K. Vannucci, C. J. Dares, M. K. Coggins, T. J. Meyer, *Proc. Natl. Acad. Sci. USA* **2015**, *112*, 4935 – 4940.
[36] R. Matheu, M. Z. Ertem, J. Benet Buchholz, E. Coronado, V. S. Batista, X. Sala, A. Llobet, *J. Am. Chem. Soc.* **2015**, *137*, 10786 – 10795.
[37] D. W. Shaffer, Y. Xie, D. J. Szalda, J. J. Concepcion, *J. Am. Chem. Soc.* **2017**, *139*, 15347 – 15355.
[38] N. Vereshchuk, R. Matheu, J. Benet Buchholz, M. Pipelier, J. Lebreton, D. Dubreuil, A. Tessier, C. Gimbert-Suriñach, M. Z. Ertem, A. Llobet, *J. Am. Chem. Soc.* **2020**, *142*, 5068 – 5077.
[39] M. Schulze, V. Kunz, P. D. Frischmann, F. Würthner, *Nat. Chem.* **2016**, *8*, 576 – 583.
[40] V. Kunz, M. Schulze, D. Schmidt, F. Würthner, *ACS Energy Lett.* **2017**, *2*, 288 – 293.
[41] V. Kunz, J. O. Lindner, M. Schulze, M. I. S. Röhr, D. Schmidt, R. R. Mitrić, F. Würthner, *Energy Environ. Sci.* **2017**, *10*, 2137 – 2153.
[42] F. Yu, D. Poole III, S. Mathew, N. Yan, J. Hessels, N. Orth, I. Ivanović-Burmazović, J. N. H. Reek, *Angew. Chem. Int. Ed.* **2018**, *130*, 11417 – 11421; *Angew. Chem.* **2018**, *130*, 11417 – 11421.
[43] A.-L. Meza-Chincha, J. O. Lindner, D. Schindler, D. Schmidt, A.-M. Krause, M. I. S. Röhr, R. Mitrić, F. Würthner, *Chem. Sci.* **2020**, *11*, 7654 – 7664.
[44] Y. Dong, J. Zhang, J. Ma (Shandong Normal University), CN104558050A, **2015**.
[45] Z. Liu, S. K. M. Nalluri, J. F. Stoddart, *Chem. Soc. Rev.* **2017**, *46*, 2459 – 2478.
[46] C. D. Gutsche in *Calixarenes, Vol. 1*, The Royal Society of Chemistry, Cambridge, **1989**, pp. 105 – 124.
[47] D. M. Homden, C. Redshaw, *Chem. Rev.* **2008**, *108*, 5086 – 5130.
[48] L. Wu, B. Yang, L. Xing, J. Jian, Z. Tong (Technical Institute of Physics and Chemistry, China), CN104148112A, **2014**.
[49] P. Sreedevi, J. B. Nair, P. Preethanuj, B. S. Jeeja, C. H. Suresh, K. K. Maiti, R. L. Varma, *Anal. Chem.* **2018**, *90*, 7148 – 7153.
[50] S. Chakraborty, S. G. Ramkumar, S. Ramakrishnan, *Macromolecules* **2017**, *50*, 5004 – 5013.
[51] Y. Liang, S. Liu, R. Wang, J. Liu, K. S. Chichak (General Electric Company, USA), WO2010151389A1, **2010**.
[52] F. Li, B. Zhang, X. Li, Y. Jiang, L. Chen, Y. Li, L. Sun, *Angew. Chem. Int. Ed.* **2011**, *50*, 12276 – 12279; *Angew. Chem.* **2011**, *123*, 12484 – 12487.
[53] L. Duan, A. Fischer, Y. Xu, L. Sun, *J. Am. Chem. Soc.* **2009**, *131*, 10397 – 10399.
[54] T. Arimura, H. Kawabata, T. Matsuda, T. Muramatsu, H. Satoh, K. Fujio, O. Manabe, S. Shinkai, *J. Org. Chem.* **1991**, *56*, 301 – 306.
[55] Y. Jiang, F. Li, F. Huang, B. Zhang, L. Sun, *Chin. J. Catal.* **2013**, *34*, 1489 – 1495.
[56] J. J. Concepcion, D. K. Zhong, D. J. Szalda, J. T. Muckerman, E. Fujita, *Chem. Commun.* **2015**, *51*, 4105 – 4108.
[57] J. An, L. Duan, L. Sun, *Faraday Discuss.* **2012**, *155*, 267 – 275.
[58] L. Duan, L. Wang, A. K. Inge, A. Fischer, X. Zou, L. Sun, *Inorg. Chem.* **2013**, *52*, 7844 – 7852.
[59] M. V. Sheridan, B. D. Sherman, Z. Fang, K.-R. Wee, M. K. Coggins, T. J. Meyer, *ACS Catal.* **2015**, *5*, 4404 – 4409.
[60] V. Kunz, V. Stepanenko, F. Würthner, *Chem. Commun.* **2015**, *51*, 290 – 293.
[61] L. Francàs, X. Sala, J. Benet Buchholz, L. Escriche, A. Llobet, *ChemSusChem* **2009**, *2*, 321 – 329.
[62] B. Radaram, J. A. Ivie, W. M. Singh, R. M. Grudzien, J. H. Reibenspies, C. E. Webster, X. Zhao, *Inorg. Chem.* **2011**, *50*, 10564 – 10571.
[63] P. Garrido-Barros, C. Gimbert-Suriñach, R. Matheu, X. Sala, A. Llobet, *Chem. Soc. Rev.* **2017**, *46*, 6088 – 6098.
[64] J. J. Concepcion, J. W. Jurss, J. L. Templeton, T. J. Meyer, *J. Am. Chem. Soc.* **2008**, *130*, 16462 – 16463.
[65] F. Liu, J. J. Concepcion, J. W. Jurss, T. Cardolaccia, J. L. Templeton, T. J. Meyer, *Inorg. Chem.* **2008**, *47*, 1727 – 1752.
[66] Z. Chen, J. J. Concepcion, X. Hu, W. Yang, P. G. Hoertz, T. J. Meyer, *Proc. Natl. Acad. Sci. USA* **2010**, *107*, 7225 – 7229.
[67] D. Moonshiram, V. Purohit, J. J. Concepcion, T. J. Meyer, Y. Pushkar, *Materials* **2013**, *6*, 392 – 409.
[68] F. Li, K. Fan, L. Wang, Q. Daniel, L. Duan, L. Sun, *ACS Catal.* **2015**, *5*, 3786 – 3790.
[69] F. A. Carey, R. J. Sundberg, *Advanced Organic Chemistry: Part A: Structure and Mechanisms*, Springer, **2007**.
[70] N. Iordanova, S. Hammes-Schiffer, *J. Am. Chem. Soc.* **2002**, *124*, 4848 – 4856.
[71] S. Hammes-Schiffer, A. A. Stuchebrukhov, *Chem. Rev.* **2010**, *110*, 6939 – 6960.
[72] S. Hammes-Schiffer, *J. Am. Chem. Soc.* **2015**, *137*, 8860 – 8871.
[73] J. S. Kretchmer, T. F. Miller, *Inorg. Chem.* **2016**, *55*, 1022 – 1031.
[74] A. R. Parent, R. H. Crabtree, G. W. Brudvig, *Chem. Soc. Rev.* **2013**, *42*, 2247 – 2252.
[75] B. Limburg, E. Bouwman, S. Bonnet, *ACS Catal.* **2016**, *6*, 5273 – 5284.
[76] A. Juris, V. Balzani, F. Barigelletti, S. Campagna, P. Belser, A. von Zelewsky, *Coord. Chem. Rev.* **1988**, *84*, 85 – 277.
[77] A.-L. Meza-Chincha, D. Schindler, M. Natali, F. Würthner, *ChemPhotoChem* **2020**, https://doi.org/10.1002/cptc.202000133.
[78] P. K. Ghosh, B. S. Brunschwig, M. Chou, C. Creutz, N. Sutin, *J. Am. Chem. Soc.* **1984**, *106*, 4772 – 4783.
[79] L. Francàs, R. Matheu, E. Pastor, A. Reynal, S. Berardi, X. Sala, A. Llobet, J. R. Durrant, *ACS Catal.* **2017**, *7*, 5142 – 5150.
[80] M. Natali, F. Nastasi, F. Puntoriero, A. Sartorel, *Eur. J. Inorg. Chem.* **2019**, 2027 – 2039.
[81] M. Hara, C. C. Waraksa, J. T. Lean, B. A. Lewis, T. E. Mallouk, *J. Phys. Chem. A* **2000**, *104*, 5275 – 5280.
[82] H. S. White, W. G. Becker, A. J. Bard, *J. Phys. Chem.* **1984**, *88*, 1840 – 1846.

Manuscript received: October 7, 2020
Version of record online: November 26, 2020